Article title: Compressive strength properties related to microstructure of chemically blown tannin-foams

Authors: Inès Meyer zu Reckendorf [a,c], Xavier Gabrion [b], Anne Bergeret [a], Clément Lacoste [a], Didier Perrin [a], Vadym Redko [c], Mathieu Orzalesi [c]

Affiliations:

[a] Polymers Composites and Hybrids (PCH), IMT Mines Ales, 30100 Ales, France

[b] Université Marie et Louis Pasteur, SUPMICROTECH, CNRS, institut FEMTO-ST, 25000 Besançon, France

[c] SEGULA Technologies, 69200 Vénissieux, France

Corresponding author: Inès Meyer zu Reckendorf

ines.meyer-zu-reckendorf@mines-ales.fr

Abstract

Biophenolic foams are of great interest in many applications for their renewability and lightness. In this paper, five formulations of tannin-foams produced via chemical foaming using harmless reactants such as tannins, hexamine and a non-toxic blowing agent are prepared and characterized. Foams with apparent density varying from 0.072 to 0.087 g/cm^3 have been obtained. The study focuses on the influence of the surfactant and the blowing agent on the physical properties of these foams. First, foam microstructure is analyzed by determining mean window diameter thanks to SEM image treatment and mean cell wall thickness, mean cell diameter, cellular porosity and internal cell wall porosity thanks to X-ray tomography. Results show an average window diameter that ranges from 132 µm to 192 µm. Average cell diameter is ranging from 603 to 985 µm and wall thickness from 55 to 70 µm. Mechanical properties, in terms of compressive strength, have been determined and a maximum elastic modulus of 2 MPa and a maximum compressive strength of 105 kPa have been obtained for 1.5 %w of blowing agent. Microstructure analysis showed that these results in the most homogeneous and the finest cell size distribution. In addition, compressive strength is influenced more by the size of the cells, windows, and walls than by how apparently dense the material appears.

Keywords: foams, tannins, biobased, microstructure, compressive strength.

Highlights:

- Tannins have been used as major source in phenolic foams.
- Characterization of opened porosity through X-ray tomography.
- Cell size distributions depend on the content in blowing agent or surfactant.
- Dependance of maximum cell diameter on compressive strength.

1. Introduction

Phenolic foams are a specific type of thermosetting foam. Phenolic foams currently on the market are oil based, as phenol, formaldehyde and blowing agents used in their production are non-renewable and continue to be depleted. Phenolic foams are mainly used as insulating materials in refrigeration and heating systems or in buildings [1]. They are also thermally stable and do not drip in the event of fire, which is of interest in the construction industry [2].

Phenolic foams are industrially formulated by mixing a resol-type phenolic resin, a surfactant, a blowing agent and a curing agent. The mixture is then poured into a mold and cured at temperatures generally between 75 and 85°C. Both open and closed molds can be used [3]. Foaming is achieved using physical or chemical blowing agents. The most widely used method is physical foaming, which involves evaporating a low-boiling solvent. Pentane is the most widely used blowing agent in phenolic foam production, while cyclopentane, hexane and petroleum ethers are less widely used [2].

It is currently necessary to find sustainable and economically viable alternatives to these polluting and harmful reagents. Biomass represents the most suitable, abundant and renewable alternative to petroleum for the manufacture of foams. Tannins are an example of non-carcinogenic polyphenolic molecules derived from biomass that could replace phenol. They are produced in almost all parts of the plant: seeds, roots, bark, wood and leaves. There are two main classes of tannins: hydrolyzable tannins, such as gallo-tannins and ellagi-tannins, and condensed polyflavonoid tannins [4]. The focus here is on the condensed tannins of mimosa (*Acacia mearnsii*). Tannins have been extensively studied as wood adhesive applications [4], [5], [6]. In addition, open-cell tannin foams have also been formulated for acoustic insulation [7], [8] or to produce carbonized tannin foams [9], [10] for many different applications.

In this work, different formulations of tannin-foam are tested, varying the blowing agent content and the surfactant type and content. Thus, chemical composition of the foam varies and this implies a potential modification of reticulation or expansion behavior and finally microstructure. Foam microstructure is often observed thanks to scanning electron microscope (SEM). They have a random cell shape and their morphology can be closed, opened or mixed. Open-cell porosity implies the existence of windows in the cells covered by a film sometimes destroyed, whereas closed-cell porosity is an assembly of solid walls [11]. Cells are characterized by their diameter and wall thickness. For instance, conventional polyurethane foams have relatively large cell sizes (greater than 300 µm) with thick walls (greater than 5 µm) and a density between 103 and 106 cells/cm^3 [12].

Currently different techniques are used to reach cell diameter or total porosity of open-cell tannin-based foams. Several works are based on SEM or optical microscopy image treatments [13], [14], [15]. By this way, Szczurek et al. determined average window diameter thanks to SE (secondary electron) and BSE (backscattered electrons) SEM observations of carbon-coated tannin-foams at various magnifications. They reported that SE are more relevant for estimating average cell diameters and BSE for observing the average windows diameters [16]. In other studies X-ray Computed tomography (XCT) is employed to determine cell size, cell wall and porosity of tannin-based foams [17], [18], [19]. Authors highlighted that SEM results are more probable to give biased towards large cell sizes compared to XCT, which gives more accurate average cell size [19]. On the one hand, SEM provides high-resolution images, however this gives two-dimensional information. On the other hand, XCT has a lower resolution but provides three-dimensional information. Nevertheless, the random organization of cells, the heterogenic cell distribution and the SEM images contrast may complicate the measurement of cell or window diameters. Thus, this paper proposes a new way to reach average window diameters by using SEM images of foams via a trained algorithm thanks to Cellpose$^©$ software that was detailed in a recently submitted paper [20].

In this paper, five formulations of chemically blown tannin foams are proposed and their microstructure are analyzed thanks to SEM/Cellpose$^©$ observations for window diameter measurements and to X-ray tomography for total porosity, cell diameters and wall thickness determinations. Mechanical properties, i.e. compressive strength, are also evaluated. The aim is to understand the influence of chemical variations in tannin-foams formulations on either the microstructure or the mechanical behavior.

2. Materials and methods

2.1. Reactants

Mimosa ME tannins from SCRD (Le Havre, France) has been used as a biobased polyphenolic source. The tannin species is *Acacia mearnsii*. Tannin powder has been obtained thanks to aqueous extraction from bark, concentration, purification and finally atomization. It is a beige-pink powder, soluble in water and ethanol. The pH of a 10% tannin solution is 5.0 ± 1.0. According to MALDI-TOF-MS analyses, mimosa tannins are predominantly prorobinetinidines [21].

Hexamethylenetetramine (hexamine) (purity > 99%) and p-toluenesulfonic acid monohydrate (PTSA) (purity 97%) are both provided by ThermoFisher Scientific Alfa Aesar (Kandel, Germany). The biobased and non-ionic Surfactant A, the non-ionic Surfactant B (viscosity of 600-700 mPa.s at 25 °C) and the plasticizer are supplied by Sigma-Aldrich (Saint Quentin Fallavier, France). Surfactant A is a biosourced ethoxylated sorbitan ester based on palmitic acid. Its structure consists of a hydrophilic polyoxyethylene group with long hydrophobic hydrocarbon chains [22], [23]. It has a hydrophilic/lipophilic balance (HLB) of 15, making it rather hydrophilic. Surfactant B consists mainly of a glycerol backbone, followed by polyethylene oxide chains and ricinoleic acid moieties [24]. It has an HLB of 12-14. Finally, the blowing agent is produced by Merck (Saint Quentin Fallavier, France). It is an inorganic component that releases CO_2 and/or water in the presence of acid or temperature. All these reactants are non-carcinogenic.

2.2. Preparation of foams

The first step consists in mixing the tannins with distilled water using a household electric mixer in a polypropylene jar. The water:tannin weight ratio is 3:2.5. Then hexamine, as a solid, is added. At least 30 seconds of agitation is required to disperse the hexamine. An aqueous paratoluenesulfonic acid (pTSA) solution (1.18 $mol.L^{-1}$) is prepared in parallel. The hexamine:tannin weight ratio is equal to 0.068. This solution is added to the tannin preparation and stirred. The surfactant is then added drop by drop while stirring, along with the plasticizer additive. The mixture is then stirred more vigorously for a few minutes. Lastly, the blowing agent (at a content of 1.5 to 3%w by weight) is added at low stirring speed and stirring during a few seconds. The preparation is cured in an oven at 85°C for 24 hours. The pot is not sealed. Foaming with this blowing agent involves an initial reaction releasing CO_2. Then, during curing at 85°C, a second release of CO_2 and water takes place, creating the final expansion of the foam.

All formulations are shown in Table 1. The variables are the type and content of surfactant (A or B) varying from 5 to 9% in weight or the amount of blowing agent (1.5-3% in weight). The quantity of other reagents remains fixed.

Table 1: reactant weights and weight fractions of the formulations and nominations.

	Distilled water (W)		Mimosa tannins		Hexamine		Paratoluenesulfonic acid		Surfactant (S_A or S_B)		Plasticizer (G)		Blowing agent (B)	
	%w	g	%w	g	%w	g	%w	g	%w	g	%w	g	%w	g
S_A5B1	46.3	30	38.6	25	2.6	1.7	1.7	1.12	4.6 (S_A)	3	4.6	3	1.5	1
S_A5B2	45.9	30	38.3	25	2.6	1.7	1.7	1.12	4.6 (S_A)	3	4.6	3	2.3	1.5
S_A5B3	45.6	30	38.0	25	2.6	1.7	1.7	1.12	4.6 (S_A)	3	4.6	3	3.0	2
S_A9B2	43.9	30	36.6	25	2.5	1.7	1.6	1.12	8.8 (S_A)	6	4.4	3	2.2	1.5
S_B9B2	43.9	30	36.6	25	2.5	1.7	1.6	1.12	8.8 (S_B)	6	4.4	3	2.2	1.5

2.3. Density

For each foam sample, the apparent density ρ_{app} is measured. It is calculated as the ratio between the mass of a foam sample and its volume. The weight of the foam samples is measured using a balance (Sartorius, BP221S) at a precision of 0.001 g. Five samples of foam are weighed for each formulation. These samples are parallelepipeds with dimensions of 2*4*3 cm^3 that have been measured with a ruler.

2.4. Environmental Scanning Electron Microscopy (SEM)

The FEI QUANTA 200 FEG environmental scanning electron microscope is used to map foam samples (e.g. 2*4*3 cm^3 where 4 is the height). Mapping consists of around 200 SEM images in BSE and SE mode. The images are taken parallel to the expansion direction of the foam. The observed surface is defined to delimit the area to be covered by 2 points, top left and bottom right. The magnification of each image is x100. Electron beam energy is 12.5kV. From BSE images, window density can be calculated by dividing the number of windows by the surface of an image. From SE images, a cell density can be calculated by dividing the number of cells by the surface of an image. For each formulation, more than 100 windows or cells have been counted.

2.5. Measurement of window diameter using Cellpose©

The size and distribution of the windows were determined following the procedure detailed in a recently submitted paper [20].

In brief each cell window observable in each SEM image in BSE mode is identified and separated from the image background. Windows found near the edges are suppressed from the segmentation results, as they are not fully visible and may distort the measurements. The window area is then determined and used to calculate the size of the identified window. This process is repeated for each window detected during the segmentation stage, after eliminating any windows present at the edges. The average window diameter reported is the average of each diameter found in all the images. Cellpose© software is a general-purpose artificial intelligence (AI) model capable of detecting and segmenting a wide range of objects without the need for prior parameter adjustments or additional training [25]. It has been used to reach the average window diameter. A specific model for this type of foam was developed from 195 images segmented for training and testing, evenly distributed between different foam formulations. The window contour area and equivalent diameter were determined using the Python OpenCV® library. In addition, the size of the window is approximated by calculating the equivalent diameter of a circle having the same area as the window. The equivalent diameter is calculated using the following Eq. (I):

Equation I

$$D_{eq} = \sqrt{\frac{4.\,area_{window}}{\pi}}$$

For each formulation, more than 100 SEM images in BSE modes have been tested with the described trained algorithm.

2.6. X-Ray Tomography

The experiments were carried out using a RX Solutions EasyTom tomograph equipped with an 160kV X-ray source. The tube voltage and current have been set at 60kV and 87µA respectively. The foam volume was scanned every 0.25° over 360° using a 2530DX detector at a voxel size of 2.5µm at a frame content of 1Hz (resulting in 40min of per tomography). The entire volume of 4.5*4.5*3.2 mm^3 was reconstructed using Xact software and filtered backprojection algorithm resulting in 1200 slices. These slices were analyzed using VGstudiomax© software. To highlight the homogeneity of each foam formulation, cell morphology and porosity have been evaluated as a function of the localization in the foam sample, i.e. at the top, in the middle called centre and at the bottom. For each region, and each formulation, an approximate volume of 30 mm^3 has been scanned and one measurement has been performed. For each sample, 3 planes are observed (xy, yz, xz).

These measurements enable to reach wall thickness, mean cell diameter, cellular porosity and internal wall porosity. The average values are calculated by the mean of top, middle and bottom of each sample.

To treat these data different workflows are used :

- A segmentation based on gray level was used to extract the foam from the air.
- Extraction of a Region Of Interest (ROI) and applying a closure of 3 and erode of 0.5 to extract only the wall thickness.
- A new segmentation was done from this ROI. The cellular porosity is then calculated as the Volume of ROI dived by the volume of the entire tomography.
- A wall thickness analysis in spherical method (implemented in VGstudiomax© software) was performed in the ROI to measure the wall thickness in the volume.
- In this ROI an analysis of porosity (implemented in VGstudiomax© software) based on gray level was realized to extract the internal wall porosity.

2.7. Compressive strength

A compression assembly is adapted to a Zwick machine and the ISO844:2021 standard. A 2.5 kN force load cell is used, at a speed of 10% deformation per min with a preload of 0.2 kN. Ten samples from two samples of foam are cut using a cutter and are parallelepiped in shape, with dimensions of 20*20*30 mm^3 (30 mm being the height). The samples are extracted in two columns in the center, in the expansion direction of the foam. Thus, compressive strength is studied in the expansion direction of the foam. The elastic modulus is measured in the linear part of the slope at the origin. The compressive strength at 20% deformation named σ(20%) is obtained by graphical reading. The results are given with a mean curve calculated on 10 samples and the standard deviation forms an envelope around the curve. The compressive stress σ is calculated as the measured force divided by the initial section area of the sample. The strain is calculated by dividing the relative displacement by the initial length.

3. Results and discussion

3.1. Influence of blowing agent content and surfactant type and content on tannin foam microstructure

3.1.1. *Apparent density*

Microstructural differences between formulations can be distinguished from a macroscopic perspective. Cells with larger diameters exist using higher blowing agent contents. Especially when Surfactant A is added, microstructure defaults are present on the edge of S_A5B2 and S_A9B2 samples. Figure 1 shows that tannin-foams have apparent densities ranging from 0.072 to 0.087 g/cm^3 and that the density strongly depends on the content of blowing agent. Increasing blowing agent content implies a decrease in apparent density. This has been shown with other types of foaming such as n-pentane or diethyl ether foaming [26]. These values of apparent densities are lower than those obtained by mechanical foaming without using any blowing agent, which are around 0.13-0.18 g/cm^3 [14] and much lower than those obtained by physical foaming [27]. When the Surfactant A content increases from 5 to 9 %w, apparent density increases from 0.076 to 0.084 g/cm3. In the case of S_B9B2, apparent density ranges between these two values (0.079 g/cm3).

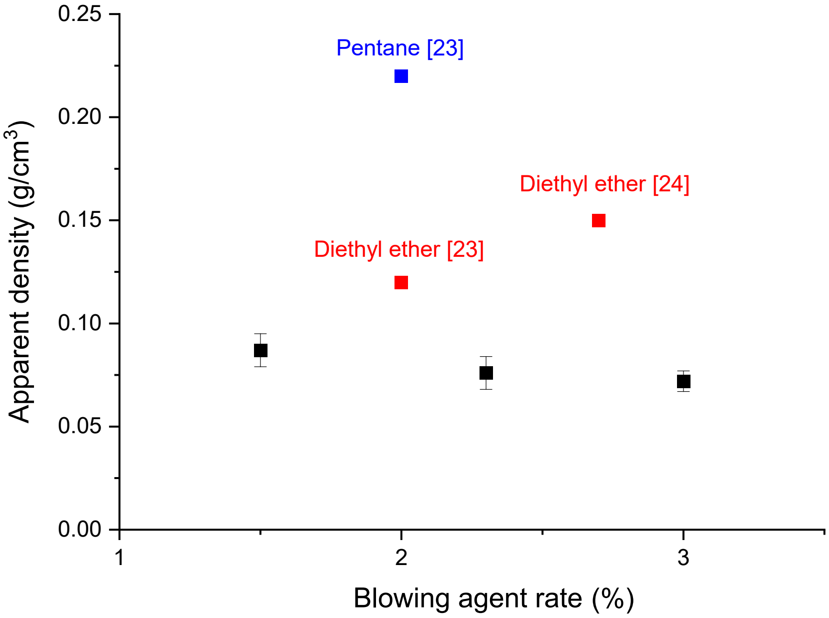

Figure 1: Influence of blowing agent content on apparent density of tannin foams compared to literature.

3.1.2. *SEM observations*

SEM observations in BSE (Figure 2) allow highlighting difference in microstructure such as window size as highlighted by Szczurek et al. [18].

Figure 2 shows an open-cell structure. As concerns S_A, it can be observed smaller windows for S_A5B1 associated to lower blowing agent content (1.5 %w) compared to S_A5B2 (2.3 %w) and S_A5B3 (3 %w). The window diameters increase when more blowing agent is added to the formulation. More CO_2 and H_2O are released in this case, implying a greater number and size of windows within the same cell. The cell size tends to increase when blowing agent content increases, because it favors the coalescence between bubbles [28], especially for S_A5B3. This also implies partially destroyed films. In fact, a low density, associated with a higher blowing agent content, favors wall opening [29]. In the case of S_B, the appearance of the cells differs from that of S_B as the cells have fewer windows. When surfactant A content increases, there is no real effect on window size at first sight.

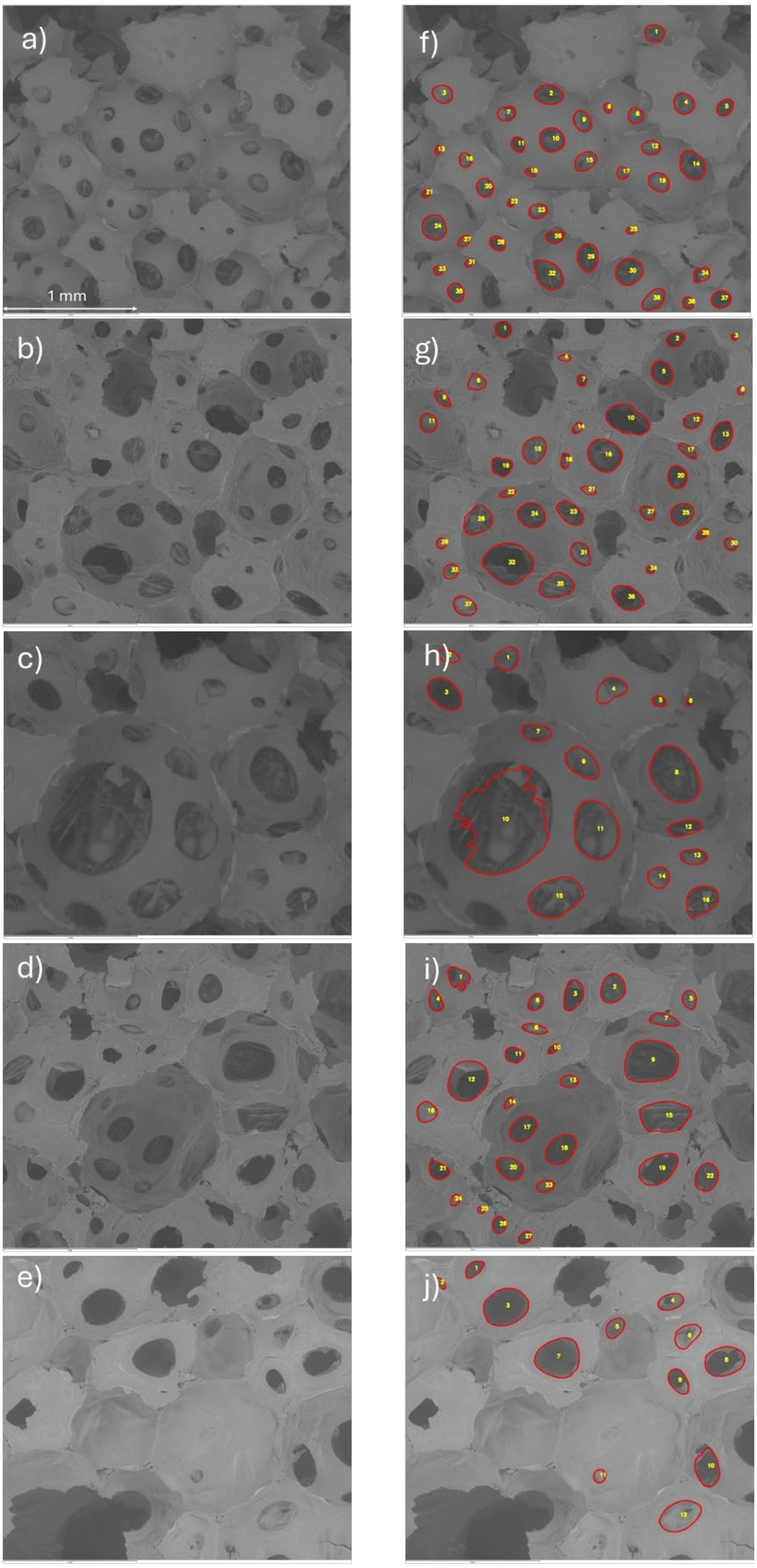

Figure 2: SEM BSE images of a) S_A5B1, b) S_A5B2, c) S_A5B3, d) S_A9B2 and e) S_B9B2 and f), g), h), i) and j) corresponding Cellpose$^{©}$ detections, the scale bar represents 1 mm for all images.

Images of the detections thanks to Cellpose© show satisfactory results (Figure 2 f), g), h), i) and j)). In fact, windows on the edge of the image and obstructed windows are not considered. Results of window diameter measurements are given in Figure 3. Results confirm that window diameter increases as blowing agent content increases in the case of S_A. In addition, increasing surfactant A content doesn't influence window size which remains around 155 µm. When comparing S_A and S_B (9 %w) for a given blowing agent content (1.5 %w), S_B9B2 has greater windows (+15%) than S_A9B2, so the surfactant nature has an influence on window diameter too.

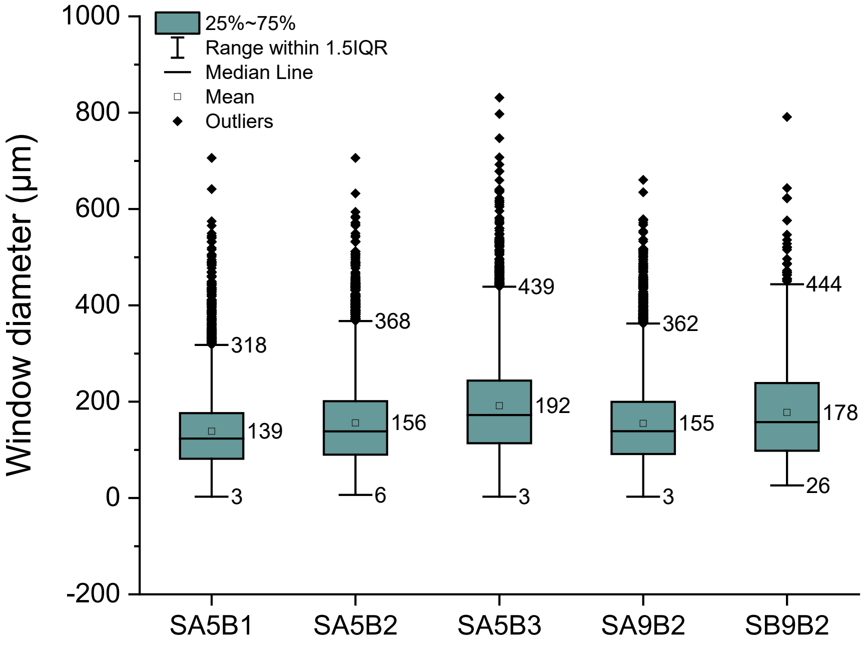

Figure 3: window diameter distributions of S_A5B1, S_A5B2, S_A5B3, S_A9B2 and S_B9B2.

3.1.3. X-Ray microtomography analysis

A deeper analysis of microstructure is enabled by X-ray microtomography. Additional information is reached such as cellular porosity, internal wall porosity, mean cell diameter and cell wall thickness. A complementary study is made on the influence of localization of the sample in the foam sample: top, centre and bottom.

3.1.3.1. Cellular porosity and internal wall porosity

3.1.3.1.1. Influence of the blowing agent content

Table 2 summarizes cellular porosity and internal wall porosity for the foams as a function of the localization when surfactant A is used. Regarding cellular porosity, it is close to 91% for the S_A5B2, S_A5B3, S_A9B2 and S_B9B2 in average. It is close to 90% for S_A5B1. Regarding internal wall porosity, values are between 15% and 38% depending on the localization. It can be noticed that there is quite a regular decrease from the bottom to the centre of the foam then from the centre to the top whatever the foam formulation. At the bottom, the internal wall porosity increases with the blowing agent ratio from 25.3% to 31.5%. At the centre and the top, the porosity variation is different with a lower value for S_A5B2 compared to S_A5B1 and S_A5B3. Moreover, the highest value of the internal wall porosity is observed with S_B whatever the localization. Regarding the average values (mean values whatever the localization), cell porosity increases by +1.7% and internal wall porosity decreases by -17.6% when the blowing agent content increases from 1.5 to 2.3 %w then cell porosity increases by +1.8% and internal wall porosity increases by +6.1%wall as the blowing agent content increases from 1 to 3%wwall. Moreover, the internal wall porosity of S_A5B2 is less homogeneous than S_A5B1 and S_A5B3. This is due to less internal wall porosity at the top

Table 2: Cellular porosity and internal cell wall porosity of S_A5B1, S_A5B2, S_A5B3, S_A9B2 and S_B9B2 at the bottom, the centre and the top of the different foams, the average value are calculated.

	S_A5B1	S_A5B2	S_A5B3	S_A9B2	S_B9B2
	S_A5B1 (bottom)	**S_A5B2 (bottom)**	**S_A5B3 (bottom)**	**S_A9B2 (bottom)**	**S_B9B2 (bottom)**
Cellular porosity (%)	88.4	91.8	90.0	91.3	91.4
Internal wall porosity (%)	25.3	31.8	31.5	19.6	37.5
	S_A5B1 (centre)	**S_A5B2 (centre)**	**S_A5B3 (centre)**	**S_A9B2 (centre)**	**S_B9B2 (centre)**
Cellular porosity (%)	88.7	90.2	90.3	90.9	91.7
Internal wall porosity (%)	26.2	21.6	27.8	20.4	33.8
	S_A5B1 (top)	**S_A5B2 (top)**	**S_A5B3 (top)**	**S_A9B2 (top)**	**S_B9B2 (top)**
Cellular porosity (%)	91.9	91.8	92.8	91.3	90.7
Internal wall porosity (%)	23.0	14.8	26.4	21.4	27.0
AVERAGE	**S_A5B1**	**S_A5B2**	**S_A5B3**	**S_A9B2**	**S_B9B2**
Cellular porosity (%)	89.7 ± 1.9	91.3 ± 0.9	91.0 ± 1.5	91.2 ± 0.2	91.3 ± 0.5
Internal wall porosity (%)	25.8 ± 0.6	22.7 ± 8.6	28.6 ± 2.6	20.5 ± 0.9	32.8 ± 5.3

3.1.3.1.2. *Influence of the surfactant nature and content*

A first comparison is made between two contents of surfactant A, which are 5 %w and 9 %w. In addition, a comparison is made between surfactant A (S_A9B2) and surfactant B (S_B9B2), at a fixed blowing agent ratio of 2.3 %w (Table 2).

Regarding cellular porosity, no difference is observed when surfactant B is used compared to surfactant A or when surfactant A content increases from 5 to 9 %w. Moreover, there is no influence of the localization in the foam, and a value close to 90% is measured.

The internal cell wall porosity decreases when surfactant A content increases and is more homogeneous for S_A9B2 than S_A5B2. The internal cell wall porosity of S_B9B2 is higher than those of S_A5B2. It is +91.3%, +65.7% and +26.2% higher for S_B9B2 than S_A9B2 at the bottom, the centre and the top respectively. The average internal wall porosity is around 21% for S_A9B2 and 33% for S_B9B2. For both formulations, the internal cell wall porosity also decreases from the bottom to the centre and from the centre to the top of the foam.

3.1.3.2. *Cell diameter and cell wall thickness*

3.1.3.2.1. *Influence of the blowing agent content*

Figure 4 assesses the mean cell diameter and the mean wall thickness included the standard deviation for the foams as a function of the localization when surfactant A is used. For S_A5B1, it can be noted that the mean cell diameter slightly increases from the bottom (563 µm) to the top (641 µm) of the foam. As concerns the mean wall thickness, it is higher at the centre of the foam (65 µm) compared the thickness at the bottom (46 µm) and the top (53 µm). In the case of S_A5B2, the mean cell diameter decreases from the bottom (831 µm) to the top (641 µm) reaching therefore the same mean cell diameter as

S$_A$5B1. The same behavior is observed for the mean wall thickness. It decreased from the bottom (65 µm) to the top (52 µm) of the foam. S$_A$5B3 has globally larger cell diameter especially at the centre (1079 µm) of the foam. Cell diameter increases from the bottom (992 µm) to the centre (1079 µm) and decreases from the centre to the top (885 µm). The mean wall thickness is also higher (66-77 µm) than S$_A$5B1 (46-65 µm) or S$_A$5B2 (52-65 µm).

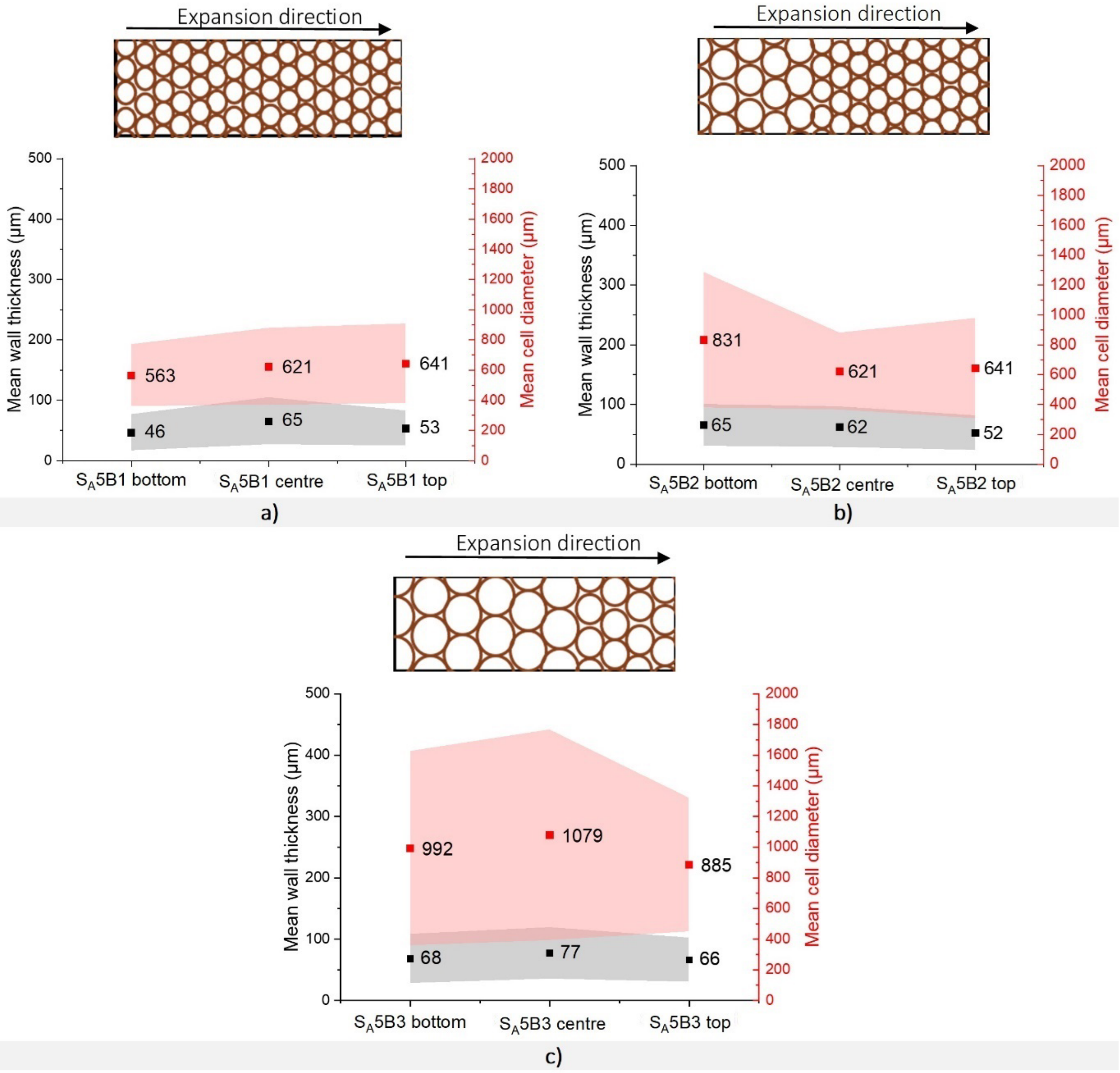

Figure 4: Mean wall thickness, mean cell diameter and schematic cell size distribution at the bottom, the centre and the top of a) S$_A$5B1, b) S$_A$5B2 and c) S$_A$5B3.

Even though the results must be put into perspective due to the small volumes of foam analyzed (around 3*3*3 mm^3 at each localization), it is possible to propose a schematic cell size distribution depending on the blowing agent ratio (Figure 4). This heterogeneity can be explained by the various destabilization phenomena occurring during foaming process and foam curing. Indeed, sedimentation has been observed at the bottom of the foam, which can lead to a higher wall thickness. Moreover, a creaming phenomenon, where bubbles go to the surface of the foam has been given evidence that may induce a higher average cell diameter. These phenomena will be deeply studied in a next paper.

3.1.3.2.2. <u>Influence of the surfactant nature and content</u>

The influence of the surfactant, either surfactant A or surfactant B, is studied on the structure, which includes mean cell walls and mean cell diameter. The role of the surfactant is to stabilize the foam by retarding the drainage from the lamellae and decreasing the resin surface tension [30]. Indeed, using different surfactants implies to change density of the foam. Thus, it modifies the foam-forming mechanism and expansion content, and consequently microstructure, especially cell size.

Regarding surfactant A, increasing its content from 5 to 9 %w implies a decrease of cell diameter from the bottom to the top of the sample (Figure 5 a) and b)). For S_A5B2, cell diameter at the bottom is around 831 µm and decreases at the top to reach 641 µm. For S_A9B2, cell diameter at the bottom is around 750 µm and decreases at the top to reach 473 µm. Regarding the cell wall thickness, for S_A5B2, it is stable between 52-65 µm. For S_A9B2, cell wall thickness is between 49-62 µm. Thus, surfactant A content is more responsible for a variation in cell diameter. Decreasing Surfactant A content enables higher cell diameter at the top, centre and bottom of the foam sample.

When surfactant A and surfactant B are compared, using the same content (9 %w), the trend in cell diameter and cell wall thickness is different. For S_B9B2, cell diameter increases from the bottom (851 µm) to the top (1071 µm). The cell wall thickness is around 63-66 µm at the bottom and the top but decreases at the centre (36 µm) of the sample. Thus, the cell wall thickness is more heterogenous when using surfactant B. This can be explained by an easier drainage for surfactant B that leads to more coalescence and air rising to form larger cells at the top. Based on these results, cell distribution schemes can be proposed.

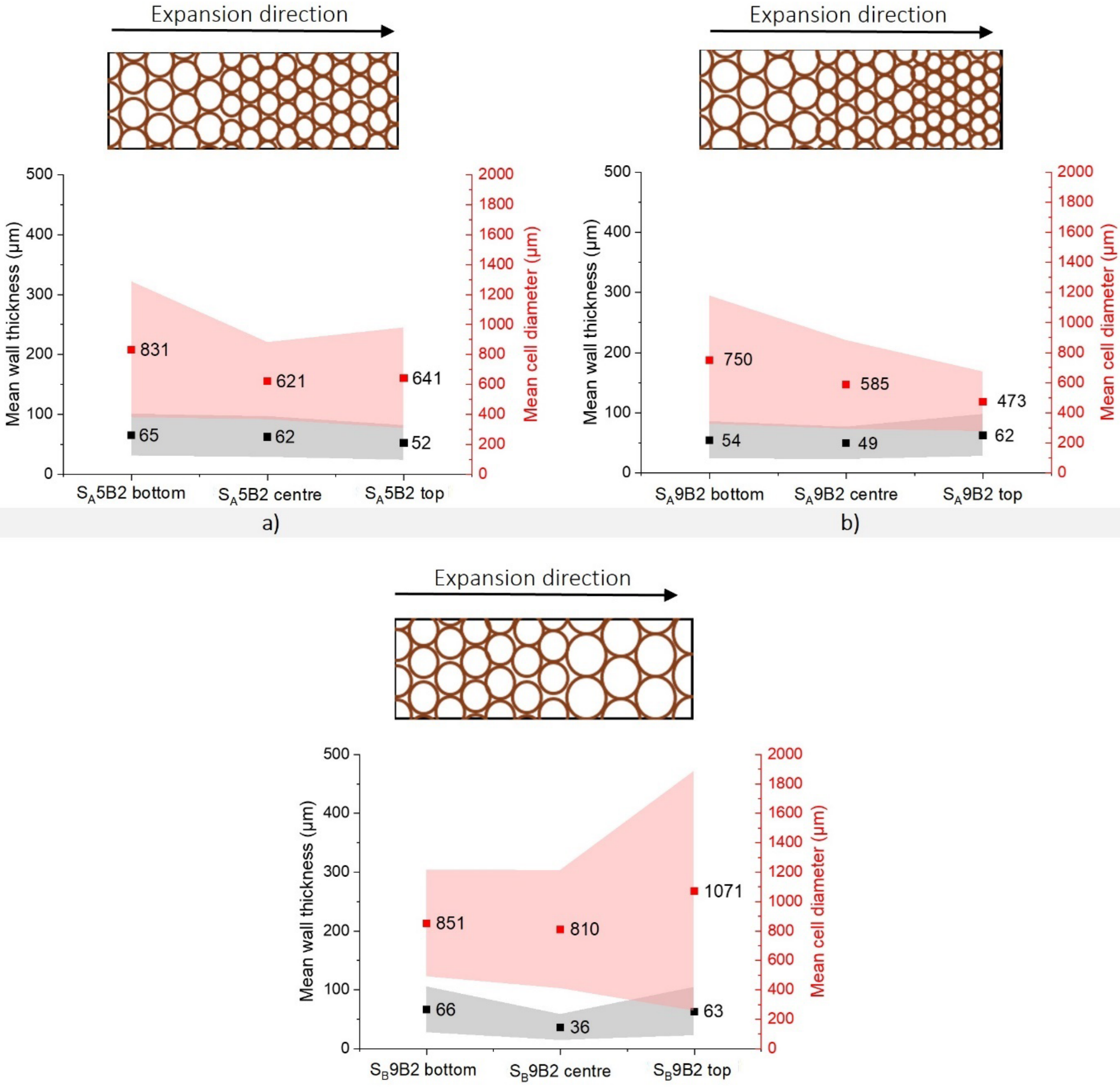

a) b)

c)

Figure 5: Mean wall thickness, mean cell diameter and schematic cell size distribution at the bottom, the centre and the top of a) S_A5B2, b) S_A9B2 and c) S_B9B2.

3.1.3.2.3. <u>3D reconstructions for a global porosity of the foam</u>

Figure 6 shows 3D tomography reconstructions of the scanned foam samples. It can be observed that the cells are spherical, and they are larger for S_B9B2 and S_A5B3 foams compared to the two others. The color gives information on wall thickness with an increase from red to blue wall. Thus, wall thickness appears to be higher for S_A5B2 and S_A5B3 foams, with more green areas.

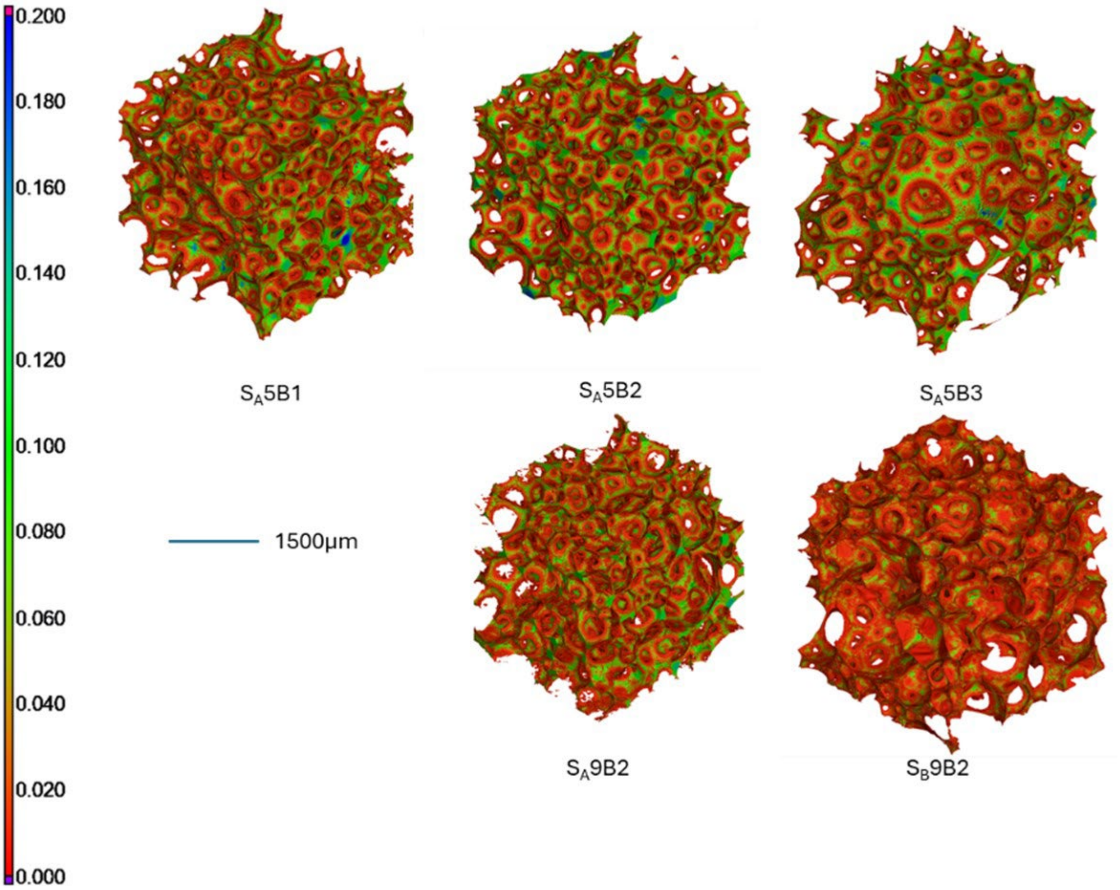

Figure 6: 3D reconstruction of X-ray tomography scanned foam samples at the centre (xz plan).

On all 5 samples, cellular porosity is around 90% (Table 4). Internal cell wall porosity is highest for S_B9B2 foam (32%). For S_A5B2, S_A5B1, S_A5B3 foams, internal wall porosity is around 25%. In addition, Table 4 shows that for a given surface, window density and cell density are higher when the blowing agent content is higher. Window and cell densities are higher for Surfactant A than Surfactant B, at a content of 9 %w.

Figure 7 gives the average values of cell diameter and wall thickness whatever the localization. Increasing blowing agent content from 1.5 %w to 3 %w implies increasing mean cell diameter from 608 to 985 µm. This reflects the fact that more CO_2 is released during the decomposition of blowing agent. It also leads to an increase of the mean cell wall thickness from 55 to 70 µm. Increasing surfactant A content, implies a decrease in cell diameter and cell wall thickness. Using surfactant B enables to increase the mean cell diameter up to 911 µm. However, the cell wall thickness remains stable at 55 µm. It should be noticed that the method used to measure cell diameters might underestimate the real size, because the technique involves growing spheres inside the cells, which could interfere with the accurate measurement of the final diameters.

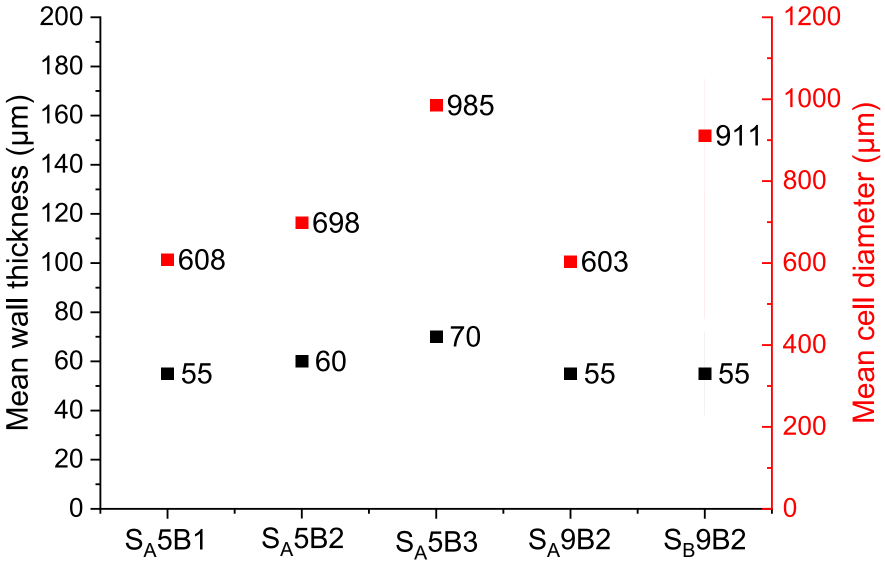

Figure 7: Mean cell wall thickness and mean cell diameter for the 5 foam formulations.

Table 3 presents a comparison of microstructure results with literature related to tannin-based foams processed through mechanical agitation. The cell diameter values obtained in this study (600-900 µm) are higher than those obtained through mechanical foaming by Merle et al. (around 100 µm) [14] or by Szczurek et al. (between 200 and 600 µm) [18].

Table 3: Comparison of microstructure results with mechanical foaming of tannin-based foams where Ø is the average diameter or thickness.

References	Resin type	Foaming process	Microstructural analysis	Results
This work	Mimosa tannins (37-39 %w)/Hexamine (2-3 %w)	Non-toxic chemical blowing agent	SEM/Cellpose©	Øwindow = 132-178 µm
			XCT	%porosity = 90-91 % Øcell = 603-911 µm Øwall = 55-70 µm
[31]	Chesnut, Mimosa tannins (24-30 %w)/Hexamine (1.5-4.4 %w)/Glyoxal (1.2-3.6 %w)	No blowing agent, mechanical agitation (500 rpm, 10 min + 1800 rpm, 30 min)	SEM/ImajeJ©	Øcell = 94-151 µm
[18]	Mimosa tannins (30-50 %w)/Hexamine (weight ratio hexamine:tannins = 0.07)	No blowing agent, mechanical agitation (500 rpm, 10 min + 2000 rpm, 20 min)	SEM/Imaje Pro Plus 6.0©	Øwindow = 50-200 µm
			XCT	%porosity = 73-97 % Øcell = 207-606 µm Østrut = 20-32 µm

It can also be observed that when cell size increases, polymer fraction in walls decreases. Indeed, intern wall porosity increases. The relationship between cell diameter and wall thickness is complex. In general, as cell diameter increases, wall thickness also increases when surfactant A is fixed. However, this trend was not observed in the tannin foams studied by Sczcurek et al., who found that decreasing cell diameter led to an increase in wall thickness [18].

3.2. Influence of the blowing agent content and of the surfactant type and content on tannin foam on mechanical properties in compression

Figure 8 shows the compression curves that are typical of brittle foams. The first part of the curve with a strain under 10% is quasi-linear. This is associated to the failure of the weakest walls and cell edges of the foam as explained by Szczurek et al. [18]. Then, after 10% deformation until around 70%, a plateau appears, associated with buckling of the cell beams. Finally, beyond 70%, there is an increase of stress values which means that the foam undergoes densification [32].

Regarding the influence of the blowing agent content, no real difference is observed on the plateau height of S_A5B2 and S_A5B3, because the apparent density is close, despite the variation in blowing agent content. The plateau is higher for S_A5B1 because apparent density is +14.5% higher compared to S_A5B2. Regarding the influence of surfactant nature, the plateau height of S_B9B2 is higher than S_A9B2 even if the apparent density is lower. Especially, σ(20%) of S_B9B2 is +7% higher than S_A9B2 and elastic modulus is +42% higher. Regarding surfactant A content, σ(20%) of S_A9B2 is +33% higher than S_A5B2 and elastic modulus is -5% higher. This is accompanied by an increase in apparent density of +11%.

Chemically blown tannin-foams of this study have lower mechanical properties than n-pentane blown tannin foams [13], [33], [34]. Indeed, Tondi et al. explored compressive strength of physically blown tannin foams. In z expansion direction, they reported compressive strength ranging from 120 to 3970 kPa associated to relative densities ranging from 0.037 to 0.306 g/cm^3 [35]. Research on mechanically blown tannin foams [8], [18], [31] also showed higher mechanical properties. Delgado-Sanchez reported compressive strength of 189 kPa ± 30 kPa and elastic modulus of 3.33 MPa ± 0.20 MPa for mechanically blown meringue-type foams with relative densities of 0.04 [8]. Merle et al. presented foams with apparent densities ranging from 0.105-0.188 g/cm^3, with an elastic modulus between 12 and 29 MPa and a compressive strength between 260 and 810 kPa [31]. Less satisfactory mechanical properties for our study may be due to the process used which is based on thermal decomposition of the blowing agent and free rise of the foam in an open mold on one hand. On the other hand, the chemical composition of the resin has an influence, such as the crosslinking agent nature (hexamine in this study). The agglomeration of tannin/hexamine particles in cell edges may weaken the structure [18]. Other crosslinking agents like formaldehyde avoid that effect, enabling higher mechanical performances.

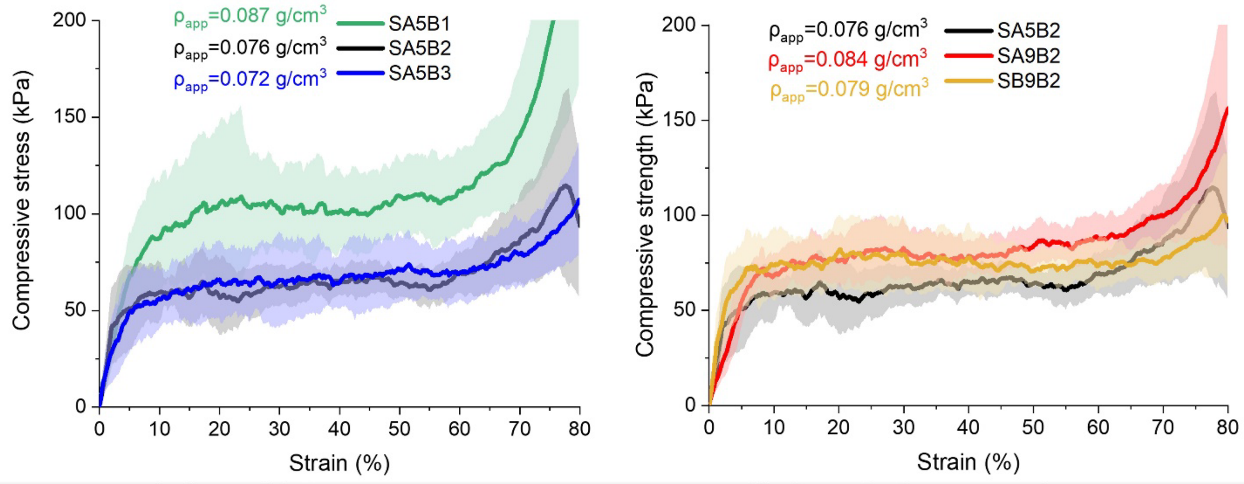

a) Influence of blowing agent content

b) Influence of surfactant nature and content

Figure 8: Compressive strength evolution as a function of strain for a) S_A5B1, S_A5B2, S_A5B3 and b) S_A5B2, S_A9B2, S_B9B2 foams showing the influence of blowing agent content and of surfactant nature. Apparent densities (ρ_{app}) in g/cm^3 are indicated for each formulation. The envelope of each mean curve corresponds to the standard deviation associated with each mean curve with corresponding colors.

Table 4 presents mechanical properties of the five foams as well as main microstructure parameters previously discussed. Elastic modulus of S_A5B2 is 24% lower than S_A5B1 and 15% lower than S_A5B3. This may be due to the lower internal wall porosity (22.7 ± 8.6 %) and the void distribution in the cell walls.

In fact, through X-ray tomography voids in the cell walls influence internal wall porosity and compressive resistance of the cell walls. Cell walls themselves can be thus considered as porous materials. Indeed Figure 9 shows clear evidence of the presence of voids in the walls (red arrows) especially for S_A5B3 and S_B9B2 that have both high internal wall porosities. This leads to a more fragile structure. In the case of S_B9B2, voids seem to improve compressive strength leading to a synergy of porosity in walls and resin type. Indeed, increasing the surfactant content leads to a reduction in the interfacial tension leading to an increase in window diameter and cell diameter, in the case of these specific surfactant weight ratios. However, increasing the surfactant content also implies an increase in apparent density. Combining these two parameters, this leads to a final increase in compressive strength properties.

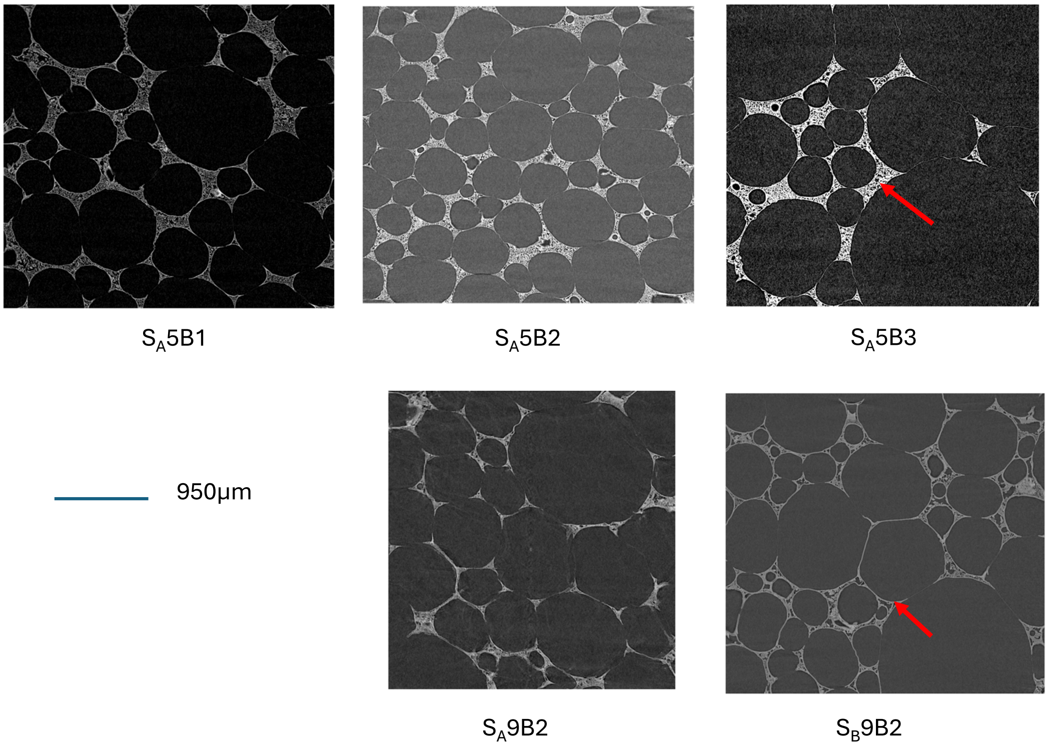

S_A5B1 S_A5B2 S_A5B3

S_A9B2 S_B9B2

Figure 9: X-ray tomography slices in the y,z plan of S_A5B1, S_A5B2, S_A5B3 and S_B9B2 at the centre of the foam.

S_A5B1 has a higher σ(20%) which is consistent with the smaller mean cell diameter (608 ± 41 µm). In fact, smaller and more uniform cell size potentially improves mechanical properties of microcellular foams [36]. The best mechanical properties can also be justified by a more homogeneous cell size distribution as shown on Figure 4 a).

Regarding the influence of surfactant A content, σ(20%) is higher for 9 %w, which is consistent with results found by [37] on tannin-furanic foams made with non-ionic surfactant. This may be linked to lower cell diameter although other microstructural parameters remain stable. However, the elastic modulus is the lowest. When both surfactant types are compared, foam microstructure is different. The mean window diameter and mean cell diameter are higher for surfactant B although cell wall thickness remains stable.

Table 4: Microstructure characterization (window, cell and porosity), apparent density, window and cell densities, elastic modulus and stress at 20% deformation of S_A5B1, S_A5B2, S_A5B3, S_A9B2 and S_B9B2 foams.

	Mean window diameter (µm)	Window density (mm^{-2})	Cellular porosity (%)	Internal wall porosity (%)	Mean cell diameter (µm)	Mean cell wall thickness (µm)	Cell density (mm^{-2})	ρ_{app} (g/cm^3)	Elastic modulus (MPa)	σ(20%) (kPa)
S_A5B1	132 ± 72	5.2	89.7 ± 1.9	25.8 ± 0.6	608 ± 41	55 ± 10	4.1	0.087 ± 0.008	2.00 ± 0.32	105.3 ± 41.5
S_A5B2	156 ± 88	4.3	91.3 ± 0.9	22.7 ± 8.6	698 ± 116	60 ± 7	2.9	0.076 ± 0.008	1.53 ± 0.55	57.1 ± 19.7
S_A5B3	192 ± 107	3.1	91.0 ± 1.5	28.6 ± 2.6	985 ± 97	70 ± 6	2.5	0.072 ± 0.005	1.81 ± 0.05	66.1 ± 20.0
S_A9B2	155 ± 85	4.9	91.2 ± 0.2	20.5 ± 0.9	603 ± 139	55 ± 7	3.8	0.084 ± 0.007	1.46 ± 0.65	76.1 ± 13.0
S_B9B2	178 ± 102	1.8	91.3 ± 0.5	32.8 ± 5.3	911 ± 140	55 ± 17	2.4	0.079 ± 0.008	2.08 ± 0.54	81.6 ± 17.7

Mechanical models such as the one proposed by Gibson and Ashby have shown that the dependence of elastic modulus, E, and compressive strength, σ, on apparent density may obey a power law (Eq. (II) and Eq. (III)) in which m and n are exponents whose values depend on the nature of the elastic forces acting within the material subjected to compression, and on the nature of the porosity, respectively [32]. This model has already been applied to tannin-foams [33].

Equation II

$$E \propto {\rho_{app}}^{m}$$

Equation III

$$\sigma \propto {\rho_{app}}^{n}$$

Figure 10 shows that elastic modulus and compressive strength at 20% of deformation do not follow the laws presented previously, compared to what Szczurek et al. explained for their mechanically blown tannin foams [18]. Celzard et al. stated that physically blown tannin foams obey Gibson and Ashby's model rather well [33].

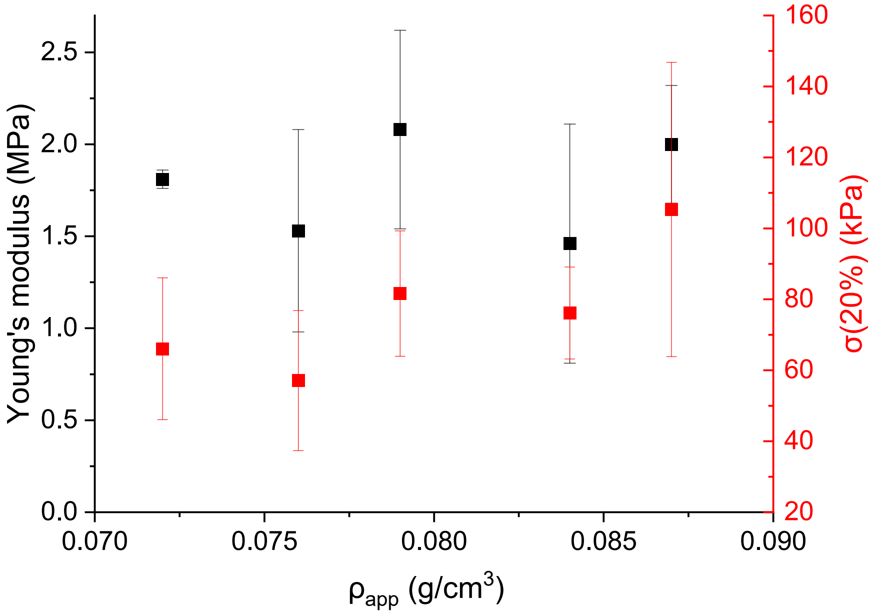

Figure 10: Evolution of elastic modulus and compressive strength at 20% of deformation as a function of apparent density of five foams.

The influence of cell and window diameters on mechanical properties has also been carried on. As apparent density is linked to cell and window diameters, the latter may have an influence on the compressive behavior of the tannin-foams. In the case of cell diameter, the maximum one is considered for each formulation because locally, a structural collapse will occur in an area with larger cells. Maximum cell diameters are close for S_A5B3 and S_B9B2. Thus, elastic modulus and σ(20%) are close too. Concerning the variation in the blowing agent content, S_A5B2 has lower elastic modulus and σ(20%) compared to S_A5B1 and S_A5B3, but the standard deviations are high so this confirms that the material is heterogeneous as seen previously due to the open-molding process allowing a free gases release and free foam expansion. Moreover, the apparent density do not significantly vary (between 0.07 and 0.09 g/cm^3) so that it should be interesting to explore other blowing agents in further investigations.

Figure 11 shows a dependence of σ(20%) and elastic modulus on characteristics of the foam microstructure such as maximum cell diameter, mean window diameter and internal wall porosity. If maximum cell diameter or mean window diameter increases, σ(20%) tends to decrease. This assumption is less true regarding elastic modulus where no trend is given in evidence. This is also the case of the dependency on window diameter. However these results must be put into perspective in view of the large standard deviations of the values. As cell diameter and wall thickness are linked by drainage phenomena, compressive strength may decrease when wall thickness increases. A relative internal cell wall porosity is calculated by dividing the internal cell wall porosity by the mean cell wall thickness and enables to evaluate the influence of the internal cell wall porosity on the mechanical properties. Elastic modulus increases when the relative internal wall porosity increases Figure 11 d), e)). This also shows little influence of surfactant A content on the elastic buckling of the walls. Surfactant B and surfactant A at same content have different effects on the elastic modulus but similar effect on compressive strength. There is no trend on the influence of the blowing agent content.

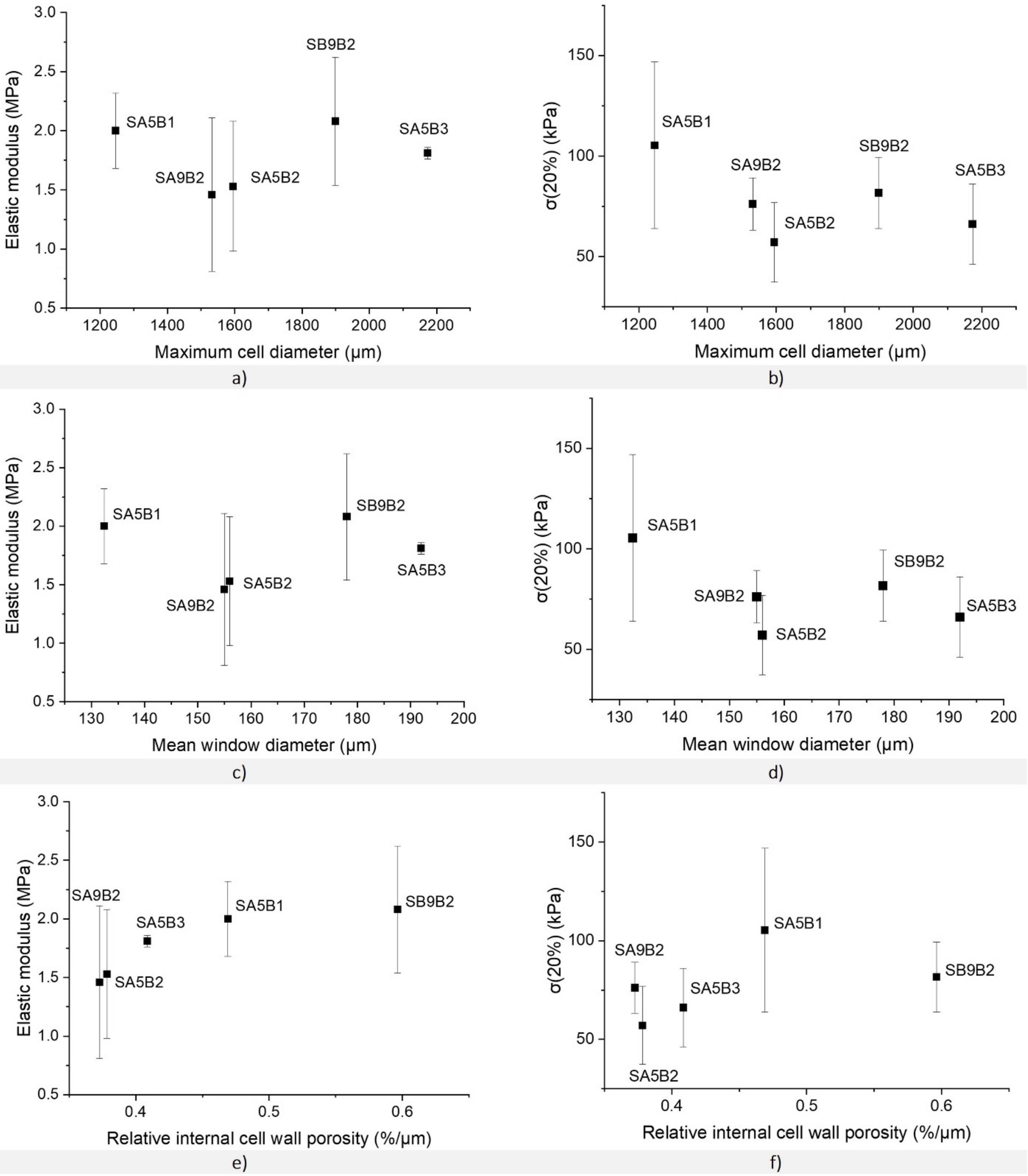

a) b)

c) d)

e) f)

Figure 11: Influence of the a) maximum cell diameter, c) mean window diameter, e) relative internal wall porosity on the elastic modulus and influence of the b) maximum cell diameter, d) mean window diameter and f) relative internal wall porosity on the compressive strength at 20% deformation.

4. Conclusion

Five chemically blown tannin-foam formulations were developed and characterized in terms of their microstructure and their compressive properties. The effects of the blowing agent content and of the surfactant type on cell and window diameters have been investigated. Thanks to an adapted Cellpose© model it has been revealed an open porosity with increasing the window diameter at higher blowing agent contents. This result has been confirmed by X-ray tomography. Cell porosity consistently hovered around 90%, increasing with higher blowing agent levels. This trend was accompanied by larger average cell diameters and thicker cell walls. Increasing Surfactant A content led to decrease cell diameter and cell wall thickness. The surfactant B notably enhanced internal wall porosity, wall thickness, and average cell diameter. However, wall thickness exhibited a complex relationship with formulation, demonstrating no clear trend across samples. Microscopic analysis of the top, the center, and the bottom sections of each foam revealed a non-uniform polymer distribution. This distribution is influenced by the apparent density, the cell size distribution, and the resin distribution within walls. Correlating compressive properties with tomographic results for these five foams, a strong relationship between the cell size and the stress at 20% of strain was observed. Higher blowing agent content led to lower compressive strength, while the surfactant B imparted added rigidity to the foams. Future studies could delve deeper into the factors influencing wall thickness and explore the potential for optimizing foam properties through tailored surfactant selection and blowing agent contents.

Acknowledgement

The authors would like to acknowledge Segula Technologies and National Association of Research and Technology (ANRT) for the financial support. XG would like to acknowledge the MIFHySTO platform for the used of Tomograph. Authors would like to thank Patrick Ienny (IMT Mines Ales) for his expertise on mechanical properties. They are also gratefully embedded to Karynn Morand (who impulses the study) and to Avigaël Ohayon (for her implication in the well-running of the study) from Segula Technologies.

Conflict of interest statement

The authors declare no conflicts of interest.

Declaration of Competing Interest

The authors declare that they have no known competing financial interests or personal relationships that could have appeared to influence the work reported in this paper.

Data availability

Data will be made available upon request.

References

[1] A. M. Borrero-López, V. Nicolas, Z. Marie, A. Celzard, and V. Fierro, “A Review of Rigid Polymeric Cellular Foams and Their Greener Tannin-Based Alternatives,” *Polymers (Basel)*, vol. 14, no. 19, Oct. 2022, doi: 10.3390/polym14193974.

[2] C. Mougel, T. Garnier, P. Cassagnau, and N. Sintes-Zydowicz, “Phenolic foams: A review of mechanical properties, fire resistance and new trends in phenol substitution,” *Polymer (Guildf)*, vol. 164, pp. 86–117, Feb. 2019, doi: 10.1016/j.polymer.2018.12.050.

[3] P. R. Sarika, P. Nancarrow, A. Khansaheb, and T. Ibrahim, “Progress in Bio-Based Phenolic Foams: Synthesis, Properties, and Applications,” *ChemBioEng Reviews*, vol. 8, no. 6, pp. 612–632, Dec. 2021, doi: 10.1002/cben.202100017.

[4] A. Pizzi, “Tannins: Prospectives and actual industrial applications,” *Biomolecules*, vol. 9, no. 8, Aug. 2019, doi: 10.3390/biom9080344.

[5] F. Santiago-Medina, G. Foyer, A. Pizzi, S. Caillol, and L. Delmotte, “Lignin-derived non-toxic aldehydes for ecofriendly tannin adhesives for wood panels,” *Int J Adhes Adhes*, vol. 70, pp. 239–248, Oct. 2016, doi: 10.1016/j.ijadhadh.2016.07.002.

[6] P. R. Sarika, P. Nancarrow, A. Khansaheb, and T. Ibrahim, “Bio-based alternatives to phenol and formaldehyde for the production of resins,” *Polymers (Basel)*, vol. 12, no. 10, pp. 1–24, Oct. 2020, doi: 10.3390/polym12102237.

[7] M. C. Basso, X. Li, V. Fierro, A. Pizzi, S. Giovando, and A. Celzard, “Green, formaldehyde-free, foams for thermal insulation,” *Adv Mater Lett*, vol. 2, no. 6, pp. 378–382, Dec. 2011, doi: 10.5185/amlett.2011.4254.

[8] C. Delgado-Sánchez, “Nouvelles méthodes d’optimisation et de caractérisation de mousses à base de tanins pour l’isolation thermique du bâtiment,” 2018. Accessed: May 20, 2025. [Online]. Available: https://theses.fr/2017LORR0246

[9] A. Szczurek, V. Fierro, A. Pizzi, M. Stauber, and A. Celzard, “Carbon meringues derived from flavonoid tannins,” *Carbon N Y*, vol. 65, pp. 214–227, Dec. 2013, doi: 10.1016/j.carbon.2013.08.017.

[10] A. Szczurek, V. Fierro, A. Pizzi, and A. Celzard, “Emulsion-templated porous carbon monoliths derived from tannins,” *Carbon N Y*, vol. 74, pp. 352–362, 2014, doi: 10.1016/j.carbon.2014.03.047.

[11] B. E. Obi, “Structure–Property Relationships of Polymeric Foams,” in *Polymeric Foams Structure-Property-Performance*, Elsevier, 2018, pp. 189–205. doi: 10.1016/b978-1-4557-7755-6.00007-0.

[12] B. E. Obi, “Fundamentals of Polymeric Foams and Classification of Foam Types,” in *Polymeric Foams Structure-Property-Performance*, Elsevier, 2018, pp. 93–129. doi: 10.1016/b978-1-4557-7755-6.00005-7.

[13] G. Tondi and A. Pizzi, “Tannin-based rigid foams: Characterization and modification,” *Ind Crops Prod*, vol. 29, no. 2–3, pp. 356–363, Mar. 2009, doi: 10.1016/j.indcrop.2008.07.003.

[14] J. Merle, M. Birot, H. Deleuze, C. Mitterer, H. Carré, and F. C. El Bouhtoury, “New biobased foams from wood byproducts,” *Mater Des*, vol. 91, pp. 186–192, Feb. 2016, doi: 10.1016/j.matdes.2015.11.076.

[15] J. Eckardt, T. Sepperer, E. Cesprini, P. Šket, and G. Tondi, “Comparing Condensed and Hydrolysable Tannins for Mechanical Foaming of Furanic Foams: Synthesis and Characterization,” *Molecules*, vol. 28, no. 6, p. 2799, Mar. 2023, doi: 10.3390/molecules28062799.

[16] A. Szczurek, A. Martinez de Yuso, V. Fierro, A. Pizzi, and A. Celzard, “Tannin-based monoliths from emulsion-templating,” *Mater Des*, vol. 79, pp. 115–126, Aug. 2015, doi: 10.1016/j.matdes.2015.04.020.

[17] J. Glinz, S. Senck, J. Kastner, and G. Tondi, “Determination of pore size distribution in Tannin- and Lignin-based foams using X- ray microcomputed tomography,” in *8th Conference on Industrial Computed Tomography*, Wels, Austria, 2018.

[18] A. Szczurek, V. Fierro, A. Pizzi, M. Stauber, and A. Celzard, “A new method for preparing tannin-based foams,” *Ind Crops Prod*, vol. 54, pp. 40–53, Mar. 2014, doi: 10.1016/j.indcrop.2014.01.012.

[19] J. Merle *et al.*, “Microstructural characterization of biobased carbon foam by means of X-ray microtomography and compared to conventional techniques,” *RSC Adv*, vol. 6, no. 98, pp. 96057–96064, 2016, doi: 10.1039/c6ra16969d.

[20] A. Mesa, I. Meyer zu Reckendorf, A. Bergeret, F. Havart, and M. Orzalesi, “Comparative study of automated pore measurement methods applied to biobased phenolic foams,” *submitted*, 2025.

[21] H. Pasch, A. Pizzi, and K. Rode, “MALDI–TOF mass spectrometry of polyflavonoid tannins,” *Polymer (Guildf)*, vol. 42, no. 18, pp. 7531–7539, Aug. 2001, doi: 10.1016/S0032-3861(01)00216-6.

[22] V. Abbot and P. Sharma, “Investigation of interactions between quercetin and Tween 80 through electrolyte induced thermodynamic approach,” in *Materials Today: Proceedings*, Elsevier Ltd, 2020, pp. 61–64. doi: 10.1016/j.matpr.2020.01.274.

[23] A. Taraba and K. Szymczyk, “Spectroscopic studies of the quercetin/rutin-nonionic surfactant interactions,” *J Mol Liq*, vol. 360, Aug. 2022, doi: 10.1016/j.molliq.2022.119483.

[24] E. J. A. Suys *et al.*, “A Nonionic Polyethylene Oxide (PEO) Surfactant Model: Experimental and Molecular Dynamics Studies of Kolliphor EL,” *J Pharm Sci*, vol. 108, no. 1, pp. 193–204, Jan. 2019, doi: 10.1016/j.xphs.2018.11.028.

[25] C. Stringer, T. Wang, M. Michaelos, and M. Pachitariu, “Cellpose: a generalist algorithm for cellular segmentation,” *Nat Methods*, vol. 18, no. 1, pp. 100–106, Jan. 2021, doi: 10.1038/s41592-020-01018-x.

[26] X. Li, A. Pizzi, C. Lacoste, V. Fierro, and A. Celzard, “Physical properties of tannin/furanic resin foamed with different blowing agents,” *Bioresources*, vol. 8, no. 1, pp. 743–752, Feb. 2013, doi: 10.15376/biores.8.1.743-752.

[27] C. Lacoste, M. C. Basso, A. Pizzi, M.-P. Laborie, D. Garcia, and A. Celzard, “Bioresourced pine tannin/furanic foams with glyoxal and glutaraldehyde,” *Ind Crops Prod*, vol. 45, pp. 401–405, Feb. 2013, doi: 10.1016/j.indcrop.2012.12.032.

[28] B. Del Saz-Orozco, M. V. Alonso, M. Oliet, J. C. Domínguez, and F. Rodriguez, “Effects of formulation variables on density, compressive mechanical properties and morphology of wood flour-reinforced phenolic foams,” *Compos B Eng*, vol. 56, pp. 546–552, Jan. 2014, doi: 10.1016/j.compositesb.2013.08.078.

[29] G. F. Smits, “Effect of Cellsize Reduction on Polyurethane Foam Physical Properties*,” *Journal of Thermal Insulation and Building Envelopes*, vol. 17, pp. 309–329, 1994, doi: 1065-2744/94/04 0309-21 $06 00/0.

[30] K. R. Denslow and G. K. Rickle, “Surfactant Effects in Phenolic Foam Resins,” *Journal of cellular plastics*, vol. 25, pp. 31–42, 1989, doi: https://doi.org/10.1177/0021955X890250010.

[31] J. Merle, P. Trinsoutrot, and F. Charrier-El Bouhtoury, “Optimization of the formulation for the synthesis of bio-based foams,” *Eur Polym J*, vol. 84, pp. 577–588, Nov. 2016, doi: 10.1016/j.eurpolymj.2016.09.044.

[32] L. J. Gibson and M. F. Ashby, *Cellular Solids. Structure and properties. Second Edition*. 1997.

[33] A. Celzard, W. Zhao, A. Pizzi, and V. Fierro, “Mechanical properties of tannin-based rigid foams undergoing compression,” *Materials Science and Engineering A*, vol. 527, no. 16–17, pp. 4438–4446, Jun. 2010, doi: 10.1016/j.msea.2010.03.091.

[34] J. Eckardt *et al.*, “Synthesis and Characterization of High-Performing Sulfur-Free Tannin Foams,” *Polymers (Basel)*, vol. 12, no. 3, p. 564, Mar. 2020, doi: 10.3390/polym12030564.

[35] G. Tondi, W. Zhao, A. Pizzi, G. Du, V. Fierro, and A. Celzard, “Tannin-based rigid foams: A survey of chemical and physical properties,” *Bioresour Technol*, vol. 100, no. 21, pp. 5162–5169, Nov. 2009, doi: 10.1016/j.biortech.2009.05.055.

[36] L. Le Barbenchon, J.-B. Kopp, J.-B. A. Kopp, and J.-B. B. Kopp, “A review on the mechanical behaviour of microcellular and nanocellular polymeric foams: what is the effect of the cell size reduction?,” *Journal of Cellular Plastics*, vol. 60, no. 5–6, pp. 301–354, 2024, doi: 10.1177/ToBeAssigned.

[37] T. Sepperer, P. Šket, A. Petutschnigg, and N. Hüsing, “Tannin-Furanic Foams Formed by Mechanical Agitation: Influence of Surfactant and Ingredient Ratios,” *Polymers (Basel)*, vol. 13, no. 18, p. 3058, Sep. 2021, doi: 10.3390/polym13183058.